Journal of the Physical Society of Japan
Vol. 78, No. 7, July, 2009, 074501


# Photon Generation by Laser-Compton Scattering Using an Optical Resonant Cavity at the KEK-ATF Electron Ring

Hirotaka SHIMIZU, Sakae ARAKI, Yoshisato FUNAHASHI, Yosuke HONDA, Toshiyuki OKUGI, Tsunehiko OMORI, Nobuhiro TERUNUMA, Junji URAKAWA, Masao KURIKI[1], Shuhei MIYOSHI[1], Tohru TAKAHASHI[1], Yasuaki USHIO[1], Tachishige HIROSE[2], Kazuyuki SAKAUE[2], Masakazu WASHIO[2], Pei GUOXI[3], and LI XiaoPing[3]

*High Energy Accelerator Research Organization (KEK), Tsukuba, Ibaraki 305-0801*
[1]*Graduate School of Advanced Sciences of Matter, Hiroshima University, Higashihiroshima, Hiroshima 739-8530*
[2]*Research Institute for Science and Engineering, Waseda University, Shinjuku, Tokyo 162-0044*
[3]*Institute of High Energy Physics, Chinese Academy of Sciences, Beijing 100049, China*

(Received January 24, 2009; accepted April 10, 2009; published June 25, 2009)

We studied $\gamma$-ray generation by the laser-Compton scattering using a Fabry–Perot optical resonant cavity at the KEK-ATF electron storage ring. The laser power was enhanced up to 388 W in the optical resonant cavity with an injection power of 7 W in the ATF operation environments. The yield of photons for a crossing of a laser pulse and an electron bunch was $3.3 \pm 0.6$, which was consistent with a numerical estimate. In this paper, we report construction, installation and future prospect toward the polarized positron generation for the International Linear Collider.

KEYWORDS: ATF, Compton, ILC, linear collider, laser, polarized beam, polarized positron, positron, storage ring
DOI: 10.1143/JPSJ.78.074501

## 1. Introduction

In the International Linear Collider (ILC) electron–positron collider, the positron source is required to supply about 3000 bunches in a millisecond and each bunch must have $2 \times 10^{10}$ positrons.[1)] Conventionally, positrons are created via electromagnetic showers by injecting high-energy electrons to thick and dense materials. However, to meet the ILC requirement, no conventional materials withstands heat deposit produced by the electromagnetic shower. One possible solution to this problem is to inject high-energy O(10 MeV) photons to relatively thin materials instead of electrons. Thus, the ILC base line design adopted the so-called undulator scheme to create intense positrons, where about 150 GeV electrons accelerated by the ILC main linac are fed into a helical undulator with a length of more than 100 m to generate photons for pair creations.[1)] Although the undulator scheme is the base line for the ILC, it is not trivial for the construction of a helical undulator with a lenght of more than 100 m. In addition, the undulator scheme needs 150 GeV electron beams to create O(10 MeV) photons; therefore, the system can be tested only after the construction of the main linac as a driving electron supplier, which may not be preferable from the R&D point of view. An optional method of creating high-energy photons for positron generation is to use laser-Compton scattering (the Compton scheme). In the Compton scheme, intense laser pulses are flushed onto electron bunches. Then, laser photons are converted to high-energy photons by elastic scattering between laser photons and electrons. The required electron energy for the Compton scheme is much lower than that for the undulator scheme. For example, if we use an infrared laser of 1 μm wavelength, a few GeV electron beam energy is sufficiently high for creating photons for pair creations by laser-Compton scattering.

The other aspect of the positron sources for the ILC is polarization. As has been demonstrated by SLC/SLD experiments,[2,3)] electron beam polarization plays a crucial role in high-energy electron–positron colliders and is also planned in ILC experiments.[1)] In addition to the electron beam polarization, it is discussed that positron beam polarization can be an additional advantage for the study of ILC physics if it is well controlled.[4)] By the undulator scheme, radiated photons are naturally polarized; thus, created positrons are also expected to be polarized by about 30%, which could be higher with further development.[1)] However, since the polarization by the undulator is determined by the geometrical arrangement of magnets, it may not be easily changed. In general, while parameters sensitive to physics processes are useful for physics analysis, their uncertainty could be sources of systematic errors in the analysis. In the SLC experiment, for example, in addition to the direct measurement of the electron beam polarization, polarization was randomly flipped pulse by pulse to avoid possible systematic errors.[2,3)] It is highly preferable that the positron beam also has such capability as well once it is polarized. In this sense, the undulator scheme might have potential disadvantages for physics analysis. Polarization in the Compton scheme can be easily controlled by the polarization of incoming laser pulses.

The generation of polarized high-energy photons and subsequent polarized positrons by the Compton scheme has been demonstrated experimentally at the extraction line of KEK-ATF.[5,6)] A price to pay for the Compton scheme is, however, the difficulty in obtaining a sufficient high-energy photon intensity due to the relatively low interaction probability of laser-electron interaction. Therefore, the next task toward the ILC is to develop techniques of generating intense photons by laser-Compton scattering. The use of an intense focused pulsed laser at the laser electron interaction point is a method of increasing photon intensity. However, the design of the Compton scheme assumes laser pulses of 0.6 J/pulse with a 160 MHz repetition rate. The construction of such an intense high-repetition laser is practically difficult. Recently, a technique of stacking a pulsed laser into an external optical resonant cavity has been developed.[7)]

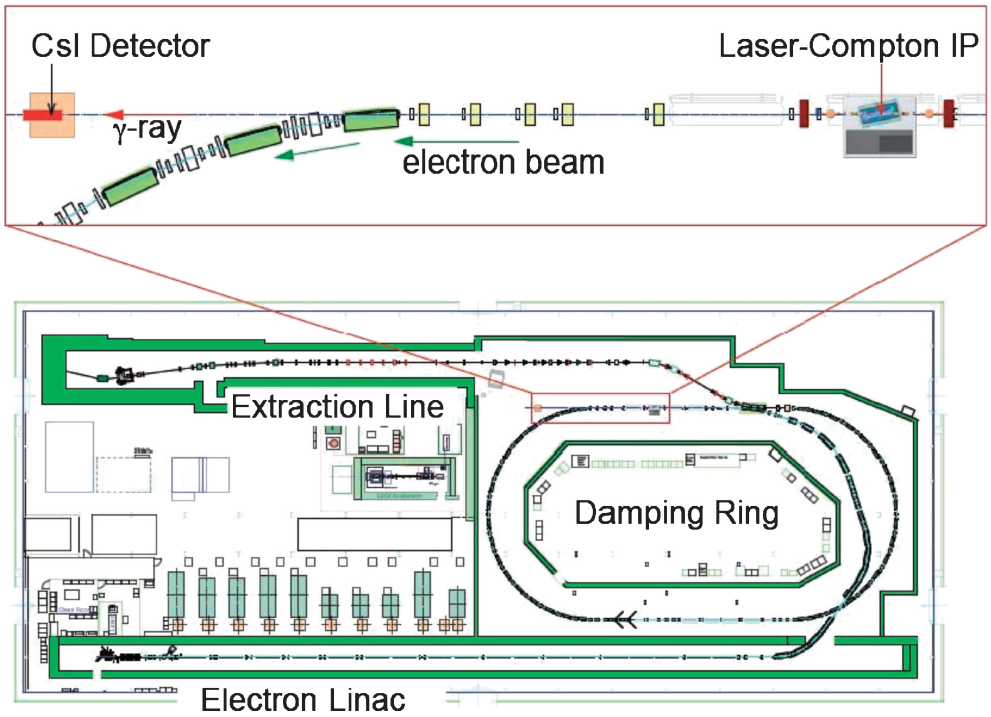


Fig. 1. KEK-ATF accelerator complex (lower figure). The upper figure shows a magnified view of the north straight section in which the positions of the optical resonant cavity and the photon detector are indicated.

Using the cavity, an enhancement of up to $O(10^4)$ may be possible, and the use of the cavity in the accelerator environment has been demonstrated for different purposes.[8] For the application of the optical resonant cavity for ILC positron sources, it may be installed in a section of an electron storage ring.[9,10] In this case, in addition to the optical requirement, there is a practical constraint or requirement for the cavity, i.e., it should not interfere with the high vacuum of the electron ring or should not affect electron beam quality. Since the optical resonant cavity is equipped with many optical and mechanical components such as mirrors and piezo actuators, meeting such a requirement is not a trivial task in a real accelerator complex. On the contrary, the accelerator environment is far from desirable for an optical system, as there are many sources of vibration, such as vacuum pumps and actuators, or many sources of electrical noise. In addition, the laser pulses in the optical resonant cavity have to be synchronized with electron bunches circulating in the accelerator while the cavity has to be resonated with laser pulses.

Regarding these situation, we performed the R&D of an optical resonant cavity with a pulsed laser at the KEK-ATF. In this article, we report the photon generation by laser-Compton scattering utilizing the optical resonant cavity in the electron storage ring, putting emphasis on design, installation and procedure of bringing the optical resonant cavity up to operation at the ATF facility.

## 2. Experimental Setup

### *2.1 Overview of the setup*

The KEK-ATF is an electron beam test facility for demonstrating the generation of ultra low emittance beams and for developing beam handling and diagnostic techniques for the ILC. As shown in Fig. 1, the accelerator complex consists of the injection linac equipped with a photocathode RF gun, a damping ring, and an extraction line. The beam energy of the ATF is 1.28 GeV and operates up to 20 bunches/train with a 2.8 ns bunch spacing. The circumference of the damping ring is about 140 m, resulting in an electron beam circulation time of about 463 ns (2.16 MHz repetition rate). At the interaction point for laser-Compton scattering, the typical beam sizes and bunch length are 100 μm (horizontal) and 10 μm (vertical) and 9 mm in the root mean square, respectively. The details of the ATF are described elsewhere ref. 11.

The optical resonant cavity for laser-Compton scattering was installed in the north straight section of the ATF damping ring. All optical devices were set on a movable table so that the laser position can be moved with respect to the electron beam with accuracies of 0.8 and 4 μm in vertical and horizontal directions, respectively. A CsI detector for the $\gamma$-ray detection is placed 15.6 m downstream of the laser electron interaction point. In between the interaction point and the CsI detector, a slit of 0.26 mrad aperture was placed to determine the energy acceptance above 16 MeV at the detector.

### *2.2 Laser pulse stacking system with the optical resonant cavity*

The schematic of the laser pulse stacking system with the optical resonant cavity is shown in Fig. 2. The laser oscillator (Time-Bandwidth COUGAR) generates laser pulses of 28 nJ/pulse with a repetition rate of 357 MHz. The wavelength and pulse width of the laser are 1064 nm and 4 ps in the root mean square, respectively. Care must be taken for the optical path between the laser and the cavity in order to match equi-phase planes at the entrance of the cavity. The optical resonant cavity is a Fabry–Perot-type

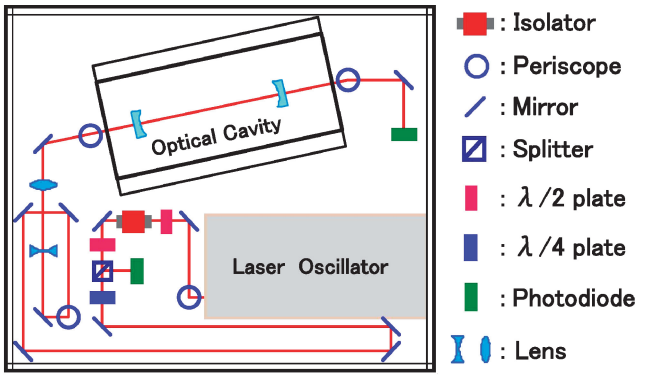


Fig. 2. Schematic of the optical system. The optical components between the laser and the optical resonant cavity are for phase matching and monitoring the resonant condition.

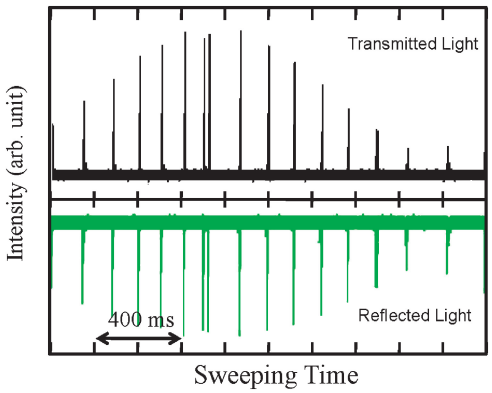


Fig. 4. Typical plot of transmitted (upper figure) and reflected (lower figure) lights from the cavity while sweeping length of the cavity by the piezoactuator.

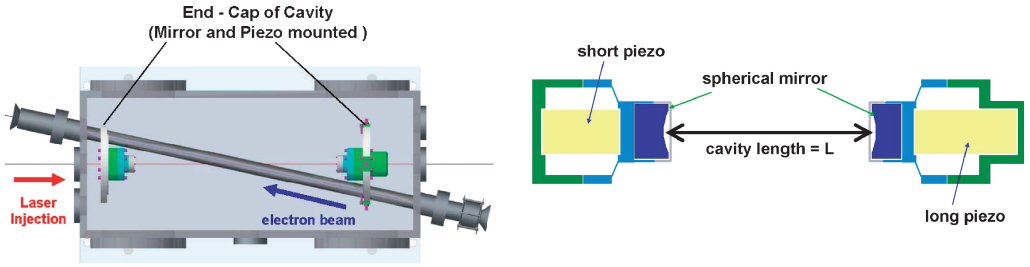


Fig. 3. Schematic of the optical resonant cavity (left) and details of the mirror attachment with piezo actuator at the end-cap part (right). Each mirror is attached to the piezo actuator via the leaf spring for fine tuning the mirror position.

cavity with spherical mirrors of 99.6% reflectivity and 210.5 mm curvature at both ends. The cavity was designed to resonate with laser pulses of 1064 nm wavelength and 357 MHz repetition. To make the resonance of the laser wave in the cavity, the length ($L$) of the cavity has to be

$$L = n\frac{\lambda}{2}, \tag{1}$$

where $\lambda$ is the wavelength of the laser, and n is a positive integer. However, pulsed lasers are not exactly monochromatic due to the uncertainty relation between pulse width and frequency. For mode-locked pulsed lasers, the spectrum has discrete Fourier components with the separation $\approx \lambda^2/2L'$ around $\lambda$, where $L'$ is the length of the cavity resonator inside the mode-locked laser oscillator. Therefore, an additional condition for the optical resonant cavity length is required in order for all the Fourier components of a laser pulse to be on resonance. The condition is expressed as

$$L = mL', \tag{2}$$

where $L'$ and $m$ are the length of the cavity resonator inside the mode-locked laser oscillator and a positive integer, respectively. We choose $L = L' = 420$ mm, which is one-half the laser pulse separation for a 357 MHz repetition rate. The optical resonant cavity is equipped with spherical mirrors of 99.6% reflectivity at both ends. The performance of the cavity in terms of the resonator is expressed by the finesse F and can be expressed under the ideal resonant condition as

$$F = \frac{\pi}{1-R},$$

where $R$ is the reflectivity of the mirror and $F \approx 790$ for the reflectivity of 99.6%. Using the finesse, the power enhancement of the laser pulse in the cavity can be estimated as $F/\pi$.

To make the cavity on resonance with the laser, the position of the mirrors can be fine-tuned by the piezoactuator, as illustrated in Fig. 3, while the resonance condition is monitored by transmitted and reflected laser pulses. A typical resonance scan obtained by changing the cavity length is shown in Fig. 4. We observed multiple peaks for both transmitted and reflected lights. The peak appears every $\lambda/2$ as the length of the cavity satisfies the condition (1). The separation of Fourier components in a laser pulse, 0.0013 nm for $L = 420$ mm and $\lambda = 1064$ nm, is too small to be resolved in the scan and resonance condition (2) can be monitored by the height of the resonant peak. The peak with a maximum height shows that all Fourier components are on resonance, i.e., both conditions were satisfied. The achieved finesse was calculated from the width and separation of the resonant peaks, and found to be 1190. This value is regarded to be consistent with the estimate from the reflectivity of the mirror as the reflectivity is a specification guaranteed by the manufacturer.

In addition to power stacking, the cavity is designed to focus laser pulses by the spherical mirrors. The waist size of the laser at the focal point inside the cavity was estimated to be 30 μm by measuring the angular divergence of the transmitted light which was consistent with the designed value calculated from the length of the cavity and the curvature of the spherical mirrors.

The circumference of the ATF ring is about 140 m; however, it exhibits a seasonal variation caused by the change in ambient temperature. Practically, it changes

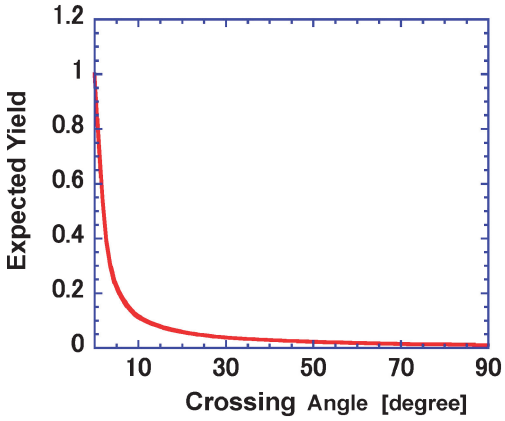


Fig. 5. Crossing angle dependence of the photon yield estimated by CAIN.[12] The yield is normalized at $\theta = 0$.

the beam repetition frequency between 356.99250 and 356.99975 MHz corresponding to a 8.5 µm difference in cavity length. One of the two piezo actuators attached to the mirror has a long stroke of 22 µm and is used to adjust the seasonal change in repetition frequency.

### 2.3 *Installation of the optical resonant cavity*

From the view point of laser Compton scattering, the head-on collision of the laser pulse and the electron bunch is preferable. However, under practical conditions, the size of the mirrors, the length of the cavity, and the size of the electron beam pipe restrict the laser-electron crossing angle. Figure 5 shows photon yield with respect to the crossing angle estimated by the CAIN, a program to simulate laser-Compton scattering.[12] We chose the crossing angle of 12°, at which the yield is about 13% of head-on collision. A slit in the electron beam pipe is inevitable to put laser pulses through the electron beam. It has to be sufficiently small so as not to interfere with the electron beam circulation inside the ring, while it has to be sufficiently large so as not to optically interfere with the laser wave inside the cavity. We estimated the effect of the slit on the performance of the cavity by numerical calculation and determined the acceptable size for the cavity. The size of the slit is 35 (w) × 5 (t) mm, which is found to be tolerable for keeping electron beam quality.

Since the optical resonant cavity has various optical components, such as mirrors, holders and piezo actuators, it potentially disturbs vacuum system. The cavity is placed in the vacuum chamber with two ion pumps of 100 L/s attached to it. As is seen on the left side of Fig. 6, the cavity has as many holes as possible while maintain rigidness and realize good air conductance between the cavity and the ion pumps. After the installation of the cavity into the damping ring, the vacuum level inside the vacuum chamber as well as the ATF ring were monitored. We found that the vacuum quality was tolerable and did not see any effect of the installation on the ATF operation. The beam conditions in terms of the lifetime and emittance of the beam were compared before and after the installation of the cavity. We did not observe any effect of the installation on the beam condition. Note that the lifetime of the electron beam in the ATF is determined by intra beam scattering and is typically 1 min.

### 2.4 *Experimental procedure and results*

To induce the collision between laser pulses and electron bunches, the laser has to be synchronized with the ATF

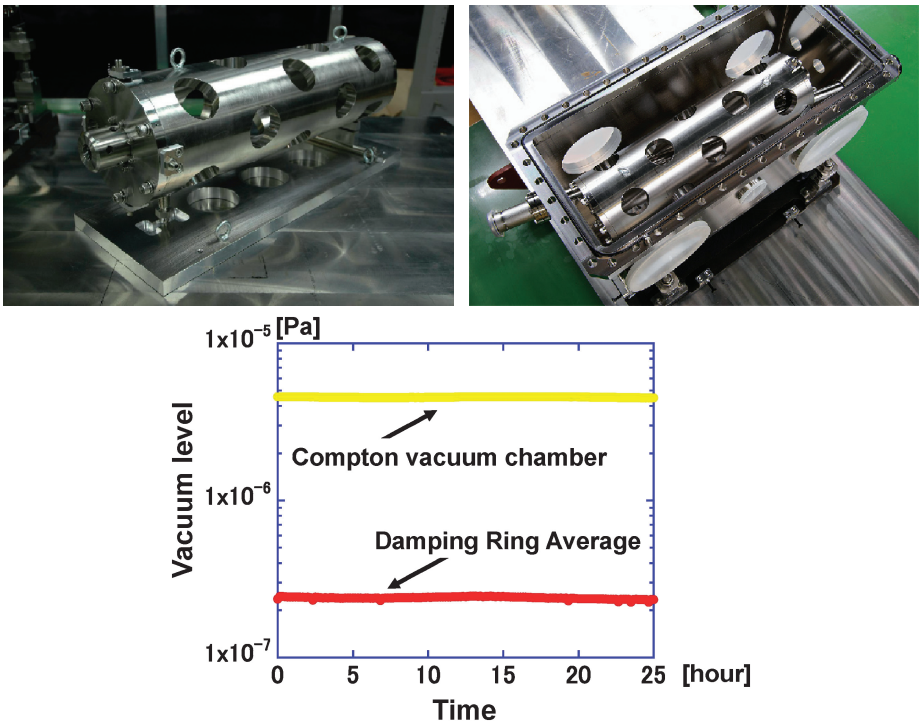


Fig. 6. Cylindrical body of the external optical resonant cavity (upper left). The upper right figure shows the body set inside the vacuum chamber. Holes on the cylindrical body improve the vacuum conductance between the cavity and the vacuum chamber. The lower figure shows the vacuum monitor after the installation of the cavity into the ATF ring. The yellow line indicates the vacuum level inside the Compton chamber, while the red one indicates that in the ATF ring. No effect of the Compton chamber on the ring has been observed.

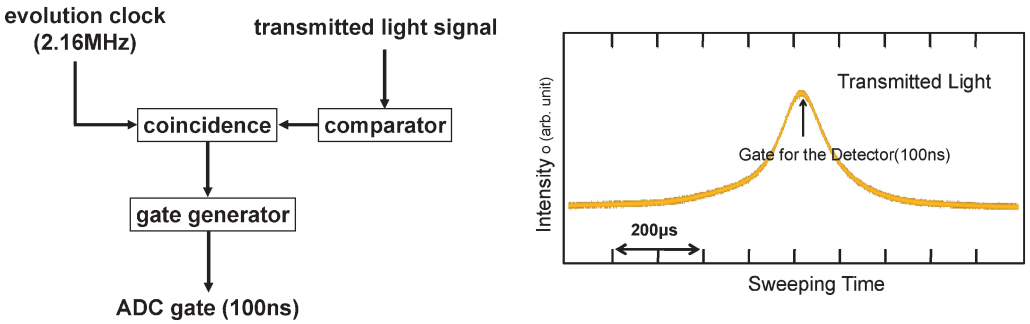


Fig. 7. Block diagram for data acquisition system (left). The gate to the ADC is open with the coincidence of the ATF timing signal and transmitted light above the threshold. The right figure shows the timing of the gate with respect to the resonant condition of the cavity.

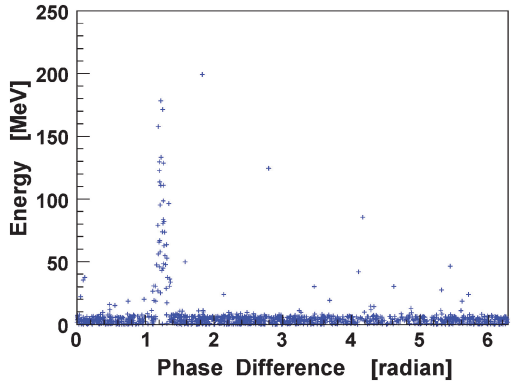


Fig. 8. Signal in the CsI detector (vertical axis) versus phase difference between the ATF master timing and the laser oscillator (horizontal axis). An excess of large signals at certain timing indicates photons from laser-Compton scattering.

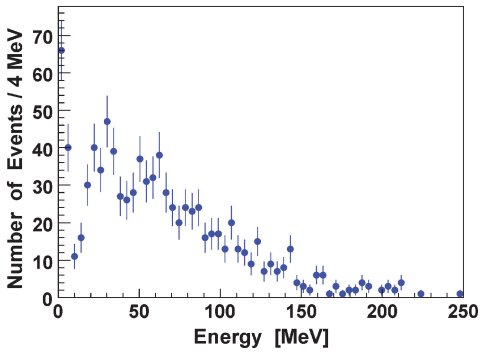


Fig. 9. Energy distribution of CsI detector after position and timing scan. Bumps at around 23 and 46 MeV correspond to the single- and double-photon events, respectively.

master oscillator. The monitor signal from the laser and the ATF master oscillator signal were fed into phase-locked system (Time-Bandwidth CLX1100), where relative timing between the laser pulses and the electron bunches can be adjusted by changing the relative phase of the two signals.

Since a system for maintaining the cavity on resonance was not implemented at the time of the installation, we continuously changed the length of the cavity using the piezo actuator and took data only when the cavity was on resonance. As illustrated in Fig. 7, it was achieved by gating the data acquisition system using the coincidence of the ATF master oscillator and the transmitted light from the cavity. The laser power stacked in the cavity during the experiment was estimated from the intensity of the transmitted light and the reflectivity of the mirror to be typically 200 to 400 W depending on the resonant condition of the cavity.

Figure 8 shows the observed signal detected by the detector while changing the relative timing between the laser pulses and the electron bunches by the phase-locked system described previously. We clearly observed the concentration of signals at a particular time which indicates photons from laser Compton scattering. A typical energy distribution observed in the detector at the time of maximum photon yield is shown in Fig. 9. The maximum energy of scattered photon in the experiment is estimated to be 28 MeV. As mentioned previously, the aperture of the slit in between the interaction point and the detector is 0.26 mr and discriminates photons above 16 MeV. Due to the finite energy resolution of the photon detector, the energy distribution of the single Compton event is smeared and observed as a Gaussian shape with an average energy and a root mean square of 23 and 6 MeV, respectively. We observed a typical Poisson-like distribution corresponding to multiple photon detection smeared by the energy distribution of the detector. The average number of photons generated in a single laser electron collision was estimated by assuming the Poisson distribution.

The average number of photons observed at each laser position relative to the electron bunch is plotted in Fig. 10 for the vertical and horizontal directions. The widths of both directions are consistent with electron bunch sizes estimated with the ATF beam parameters by taking laser spot size and collision angle of 12° into account. The timing dependence of the photon yield is plotted in Fig. 10(c) and is also found to be consistent with the bunch length of the electron beam.

The numbers of observed photons obtained with the laser and electron beam parameters are summarized in Table I. The photon yield was consistent with an estimate obtained by simulation with the laser and electron beam parameters within two standard deviations for the single bunch operation of the ATF. On the other hand, we observed an appreciable difference between photon yield and expectation for 20-bunch operation. The reason for this difference is yet to be studied; however, it might be due to the bunch-by-bunch fluctuation in timing or position, which was not previously observed in the ATF. Further investigation, such as that on the dependence of photon yield on the number of bunches, is planned in the near future.

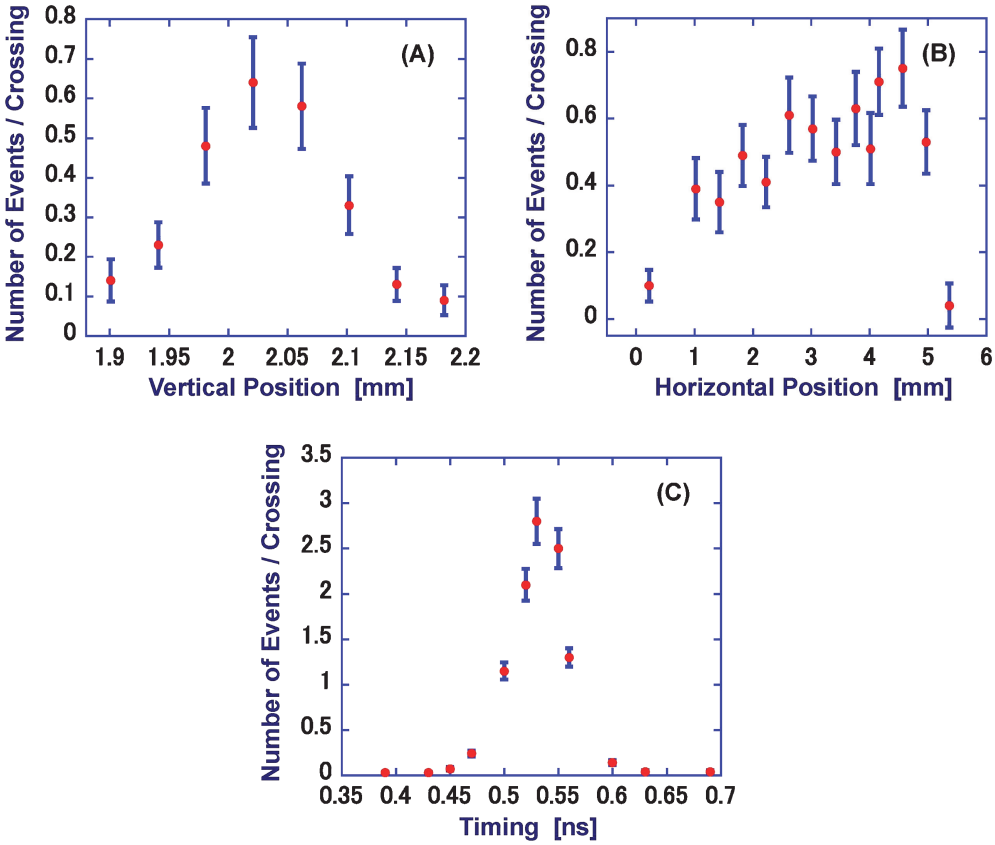


Fig. 10. Average number of photons as a function of vertical (a) and horizontal (b) positions as well as timing (c) of the laser with respect to the electron bunch.

Table I. Summary of experimental results.

| Number of bunches /train | Number of electrons /train | Stacked laser power (W) | Number of photons /laser-train crossing | Simulation |
|---|---|---|---|---|
| 1 | $7.2 \times 10^9$ | 272 | $3.3 \pm 0.6$ | 4.5 |
| 20 | $2.6 \times 10^{10}$ | 388 | $3.1 \pm 0.1$ | 20 |

## 3. Conclusion

A Fabry–Perot-type optical resonant cavity has been developed for the R&D of a polarized positron source for the ILC. This cavity has successfully been installed into the ATF electron storage ring and no interference with the ultralow-emittance electron beam in the ATF was observed. The Compton-scattered photons were observed with the optical resonant cavity system installed in the electron storage ring. The average number of photons was $3.3 \pm 0.6$ for the crossing of a single electron bunch containing $7.2 \times 10^9$ electrons and stacked laser pulses of 272 W in the cavity. The photon yield was consistent with an estimate obtained by simulation within the error for a single bunch case; however, an appreciable difference was observed in the 20-bunch operation. The reason for this difference is still under investigation, but it might indicate the existence of a new issue for the multibunch operation of the ATF beam.

For further development, an improved system is being developed in order to maintain the resonance condition of the cavity as well as to maintain the synchronization of laser pulses with the ATF. Also, more laser power stacking will be expected by using mirrors of higher reflectivity. By these developments, we expect to demonstrate an intense and stable photon yield with the optical resonant cavity system in the near future.

The positron source by the Compton scheme for the ILC assumes pulse stacking of $O(10^4)$ at the laser electron interaction points to meet the requirement described in the introduction. Based on experiences with the Fabry–Perot-type optical resonant cavity described in this paper, photon generation with a more sophisticated four-mirror ring cavity is planned at the ATF to demonstrate of photon generation for the ILC positron source.

## Acknowledgements

The authors would like to thank ATF collaborators for discussion and help with the cavity installation, particularly Dr. K. Kubo, T. Naito, H. Sakai, and M. Takano. They would also like to thank Dr. D. Howell and the extraction line laser wire group for technical help and advice. This work was supported in part by a Grant-in-Aid for Scientific Research [(B)18340076, 17GS0210], the KEK Promotion of collaborative research programs in universities, and Hiruma research funds at Hiroshima University.

1) ILC-REPORT-2007-001 (2007).
2) SLD Collaboration: Phys. Rev. Lett. **84** (2000) 5945.
3) ALEPH Collaboration, DELPHI Collaboration, L3 Collaboration, OPAL Collaboration, SLD Collaboration, LEP Electroweak Working Group, SLD Electroweak Group, and SLD Heavy Flavour Group: Phys. Rep. **427** (2006) 257.
4) G. Moortgat-Pick, T. Abe, G. Alexander, B. Ananthanarayan, A. A. Babich, V. Bharadwaj, D. Barber, A. Bartl, A. Brachmann, S. Chen, J. Clarke, J. E. Clendenin, J. Dainton, K. Desch, M. Diehl, B. Dobos, T. Dorland, H. Eberl, J. Ellis, K. Flöttmann, H. Fraas, F. Franco-Sollova, F. Franke, A. Freitas, J. Goodson, J. Gray, A. Han, S. Heinemeyer, S. Hesselbach, T. Hirose, K. Hohenwarter-Sodek, J. Kalinowski, T. Kernreiter, O. Kittel, S. Kraml, W. Majerotto, A. Martinez, H. U. Martyn, W. Menges, A. Mikhailichenko, K. Mönig, K. Moffeit, S. Moretti, O. Nachtmann, F. Nagel, T. Nakanishi, U. Nauenberg, T. Omori, P. Osland, A. A. Pankov, N. Paver, R. Pitthan, R. Pöschl, W. Porod, J. Proulx, P. Richardson, S. Riemann, S. D. Rindani, T. G. Rizzo, P. Schüler, C. Schwanenberger, D. Scott, J. Sheppard, R. K. Singh, H. Spiesberger, A. Stah, H. Steiner, A. Wagner, G. Weiglein, G. W. Wilson, M. Woods, P. Zerwas, J. Zhang, and F. Zomer: Phys. Rep. **460** (2008) 131.
5) M. Fukuda, T. Aoki, K. Dobashi, T. Hirose, T. Iimura, Y. Kurihara, T. Okugi, T. Omori, I. Sakai, J. Urakawa, and M. Washio: Phys. Rev. Lett. **91** (2003) 164801.
6) T. Omori, M. Fukuda, T. Hirose, Y. Kurihara, R. Kuroda, M. Nomura, A. Ohashi, T. Okugi, K. Sakaue, T. Saito, J. Urakawa, M. Washio, and I. Yamazaki: Phys. Rev. Lett. **96** (2006) 114801.
7) K. Takezawa: Master Thesis, Department of Physics, Kyoto University, Kyoto (2004).
8) K. Sakaue, M. Washio, S. Araki, M. Fukuda, Y. Higashi, Y. Honda, M. Takano, T. Taniguchi, J. Urakawa, N. Sasao, and H. Sakai: Proc. EPAC 2006, Edinburgh, Scotland, 2006, 07 Accelerator Technology, T22 Lasers, p. 3155.
9) M. Kuriki, S. Araki, Y. Higashi, Y. Honda, Y. Kurihara, T. Okugi, T. Omori, T. Taniguchi, N. Terunuma, J. Urakawa, M. Fukuda, K. Hirano, M. Takano, T. Hirose, K. Sakaue, M. Washio, T. Takahashi, H. Shimizu, A. Tsunemi, F. Zimmermann, H. Braun, M. Korostelev, L. Rinolfi, D. Schulte, E. Bulyak, P. Gladkikh, K. Moenigl, A. Variola, F. Zomer, X. Artru, R. Chehab, M. Chevallier, V. Strakhovenko, J. Gao, S. Guiducci, R. Raimondi, and V. Soskov: AIP Conf. Proc. **980** (2008) 92.
10) S. Araki, Y. Higashi, Y. Honda, Y. Kurihara, M. Kuriki, T. Okugi, T. Omori, T. Taniguchi, N. Terunuma, J. Urakawa, X. Artru, M. Chevallier, V. Strakhovenko, E. Bulyak, P. Gladkikh, K. Mönig, R. Chehab, A. Variola, F. Zomer, S. Guiducci, P. Raimondi, F. Zimmermann, K. Sakaue, T. Hirose, M. Washio, N. Sasao, H. Yokoyama, M. Fukuda, K. Hirano, M. Takano, T. Takahashi, H. Sato, A. Tsunemi, J. Gao, and V. Soskov: physics/0509016.
11) F. Hinode, S. Kawabata, H. Matsumoto, K. Oide, K. Takata, S. Takeda, and J. Urakawa: KEK Internal **95-4** (1995); Y. Honda, K. Kubo, S. Anderson, S. Araki, K. Bane, A. Brachmann, J. Frisch, M. Fukuda, K. Hasegawa, H. Hayano, L. Hendrickson, Y. Higashi, T. Higo, K. Hirano, T. Hirose, K. Iida, T. Imai, Y. Inoue, P. Karataev, M. Kuriki, R. Kuroda, S. Kuroda, X. Luo, D. McCormick, M. Matsuda, T. Muto, K. Nakajima, T. Naito, J. Nelson, M. Nomura, A. Ohashi, T. Omori, T. Okugi, M. Ross, H. Sakai, I. Sakai, N. Sasao, S. Smith, T. Suzuki, M. Takano, T. Taniguchi, N. Terunuma, J. Turner, N. Toge, J. Urakawa, V. Vogel, M. Woodley, A. Wolski, I. Yamazaki, Y. Yamazaki, G. Yocky, A. Young, and F. Zimmermann: Phys. Rev. Lett. **92** (2004) 054802.
12) K. Yokoya: http://lcdev.kek.jp/yokoya/CAIN/cain235/; P. Chen, G. Horton-Smith, T. Ohgaki, A. W. Weidemann, K. Yokoya: Nucl. Instrum. Methods Phys. Res., Sect. A **355** (1995) 107; P. Chen, T. Ohgaki, A. Spitkovsky, T. Takahashi, and K. Yokoya: Nucl. Instrum. Methods Phys. Res., Sect. A **397** (1997) 458.